13. Eriksson M, Ajmani SK, Mallette LE. Hyperthyroidism from thyroid metastases of pancreatic adenocarcinoma. *JAMA* 1977;238:1276–1278.
14. Bowden WD, Jones RE. Thyrotoxicosis associated with distant metastatic follicular carcinoma of the thyroid. *South Med J* 1986;79:483–486.
15. McLaughin RP, Scholz DA, McConahey WM, Childs DS. Metastatic thyroid carcinoma with hyperthyroidism: two cases with functioning metastatic follicular thyroid carcinoma. *Mayo Clin Proc* 1970;45:328–335.
16. Benua RS, Cicale NR, Sonenberg M, Rawson RW. The relation of radioiodine dosimetry to results and complications in the treatment of thyroid cancer. *Am J Roentgenol* 1962;87:171–182.
17. Mazzaferri EL. Radioiodine and other treatments and outcomes. In: Braverman LE, Utiger RD, eds. *Werner and Ingbar's the thyroid. A fundamental and clinical text*, 7th ed. Philadelphia: Lippincott-Raven; 1996:922–945.
18. Lukinac L, Franceschi M, Nöthig-Hus D, Lechpammer S, Tomasic J, Vranesic B, et al. Endogenously labeled thyroid hormones (^{131}I-T3/T4) in sera of patients with differentiated thyroid carcinoma. *Thyroid* 1996;6:201–206.
19. Hays MT, McDougall IR. Circulating ^{131}I-thyroxine and thyroid cancer. *Thyroid* 1994;4:195–198.
20. Bianchi R, Iervasi G, Matteucci F, Turchi S, Cazzuola F, Bellina CR, et al. Chromatographic identification in serum of endogenously radioiodinated thyroid hormones after iodine-131 whole-body scintigraphy in the follow-up of patients with differentiated thyroid carcinoma. *J Nucl Med* 1993;34:2032–2037.
21. Rendl J, Bier D, Blasl C, Freystadt D, Reiners C. Chromatographic identification of endogenously radioiodinated iodothyronines in urine after iodine-131 whole-body scintigraphy in the follow-up of patients with thyroid carcinoma [Abstract]. *J Nucl Med* 1997;38:267P.

FDG Imaging of Spinal Cord Primitive Neuroectodermal Tumor

Carolyn Cidis Meltzer, David W. Townsend, Sri Kottapally and Faydah Jadali
Departments of Radiology and Psychiatry, University of Pittsburgh Medical Center, Pittsburgh; and Monongahela Valley Hospital, Monongahela, Pennsylvania

PET with ^{18}F-fluoro-2-deoxy-glucose (FDG) is well established as an effective imaging modality for evaluating suspected brain tumor recurrence. Use of FDG PET imaging for spinal cord neoplasms has not yet been studied, in large part due to limitations of spatial resolution. One report of FDG PET imaging of brain involvement with primitive neuroectodermal tumor (PNET) demonstrated mild hypometabolism relative to cortical gray matter. We demonstrate with FDG PET imaging the appearance of recurrent intramedullary PNET affecting the cervical spinal cord.

Key Words: PET; spinal cord; neoplasms; primitive neuroectodermal tumor

J Nucl Med 1998; 39:1207–1209

PET has been extensively applied to the evaluation of central nervous system (CNS) neoplasms, especially high-grade glial tumors. Tumoral uptake of ^{18}F-fluoro-2-deoxy-glucose (FDG) has been shown to correlate with histological aggressivity and prognosis in both primary and recurrent gliomas (*1–5*). Hypermetabolism has also been variably reported in primary cerebral lymphoma (*6,7*), meningioma (*8*), medulloblastoma (*9*) and non-CNS brain metastasis (*10*). Relatively low glucose metabolic rates have been demonstrated in cerebral involvement with primitive neuroectodermal tumor (PNET) (*9*). Primary spinal cord PNET is uncommon and has not been previously evaluated with PET.

PET rarely has been used to assess neoplastic involvement of the spinal cord primarily due to limitations of spatial resolution and sensitivity. DiChiro et al. (*11*) demonstrated the feasibility of PET imaging with FDG for primary astrocytoma of the spinal cord. Recently, Sasajima et al. (*12*) reported visualization of a spinal cord ependymoma with ^{11}C-methionine and PET. We present the metabolic imaging features of recurrent intramedullary PNET in the cervical spine using FDG and PET.

Received Jun. 11, 1997; revision accepted Oct. 15, 1997.
For correspondence or reprints contact: Carolyn Cidis Meltzer, MD, University of Pittsburgh Medical Center, PET Facility, B-938, 200 Lothrop St., Pittsburgh, PA 15213-2582.

CASE REPORT

Patient History

The patient was a 30-yr-old man who was diagnosed with a spinal cord tumor 5 yr earlier when he presented with progressive gait disturbance. MRI of the entire spinal cord and brain was performed at that time and demonstrated extensive patchy areas of abnormal signal and expansion of the spinal cord extending from C-3 to the conus medullaris. Intraoperative biopsy of the lower thoracic spinal cord identified malignant tissue consistent with PNET. Tumor resection was performed with bilateral laminectomies from T7 through L2. The patient then received whole-brain and spine radiation followed by 6 mo of chemotherapy with vincristine and lomustine. The patient's condition remained stable for approximately 4 yr. Serial MRI studies during this interval demonstrated the persistence of mild fusiform dilatation of the cervical spinal cord from C-2 to C-7 with accompanying signal changes and posterolateral and questionable dural enhancement. The patient then presented with a new upper extremity weakness. Repeat MRI of the brain and cervical, thoracic and lumbar spine regions was unchanged with the exception of minimally increased fusiform expansion of the cervical cord and prominence of posterior dural enhancement (Fig. 1). An FDG PET scan was performed to evaluate possible recurrent tumor in the cervical spine.

After the PET scan, which indicated recurrent tumor in the cervical spinal cord, the patient underwent additional radiation treatment of the cervical spine and brain stem areas. The patient steadily deteriorated neurologically and died approximately 1 yr after the PET scan. A limited autopsy confirmed involvement of the cervical spinal cord, as well as corpus callosum, midbrain, medulla and hippocampus, with PNET. Intraventricular tumor was also demonstrated in the lateral ventricles.

PET Imaging

PET imaging was performed on an ECAT ART (CTI PET Systems, Knoxville, TN), which had an in-plane spatial resolution of approximately 6 mm and an axial resolution of 5 mm. The ART comprises two arrays of bismuth germanate block-detectors rotating at 30 rpm, and the scanner had no septa, acquiring and reconstructing data three-dimensionally. The patient was positioned in the scanner with his neck in the 16-cm field of view, and a 15-min transmission scan was performed before intravenous

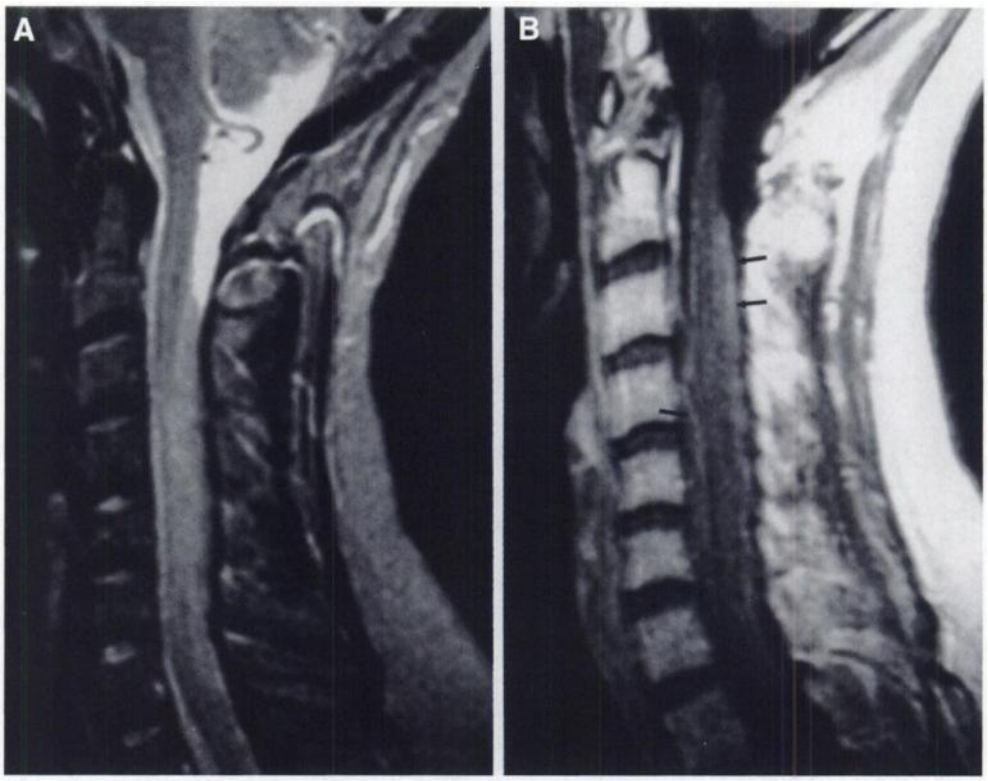

FIGURE 1. MRI of cervical spine. T2-weighted (echo time = 80; repetition time = 2000) (A) and T1-weighted (echo time = 15; repetition time = 400) after intravenous administration of gadolinium-DTPA (0.1 mmol/kg). (B) Sagittal MR images demonstrate long segment of fusiform dilatation of spinal cord with increased T2 signal and peripheral enhancement (arrow).

injection of 7 mCi FDG. Emission scanning was commenced immediately after the FDG injection, according to an acquisition protocol of 5 × 2 min, 4 × 5 min and 3 × 10 min, for a total duration of 1 hr. The last three frames, acquired from 30–60 min, were summed to form a single, 30-min image, reconstructed and displayed as sagittal sections. A single 3.5-mm-thick midsagittal section through the cervical spinal cord is shown in Figure 2A. The reconstructed spatial resolution (using a Hanning filter with a cutoff at 80% of Nyquist) was approximately 8 mm in all three spatial directions.

The image showed a focal area of markedly increased FDG uptake along the cervical spine, in agreement with the fusiform cord dilation and enhancement seen on the MRI. As expected, intense FDG uptake was also seen in the base of the cerebellum. A standardized uptake value (SUV) of 3.4 was calculated by placing an approximately 1-cm diameter circular region of interest (ROI) over the area of tumor uptake and according to the following formula:

$$\text{SUV} = \frac{\text{Mean ECAT cps/pixel} \times \text{ECF (mCi/g/ECAT cps/pixel)}}{\text{Injected dose (mCi)/body weight (g)}} \qquad \text{Eq. 1}$$

where ECF is the ECAT calibration factor to SUVs for cervical spinal cord above and below this area ranged from 1.7 to 2.0.

The complete dynamic image sequence was reconstructed and time-activity curves were obtained for ROIs placed on the carotid arteries, a section of spinal cord that appeared to show normal FDG uptake, the lesion with increased FDG uptake and the base of the cerebellum in the field of view. The time-activity curves, plotted in Figure 2B for the lesion, normal spinal cord, cerebellum and blood (carotid arteries), demonstrate uptake of FDG in the lesion to be comparable to that in the brain (cerebellum) and approximately 2–3 times that of an unaffected region of the spinal cord.

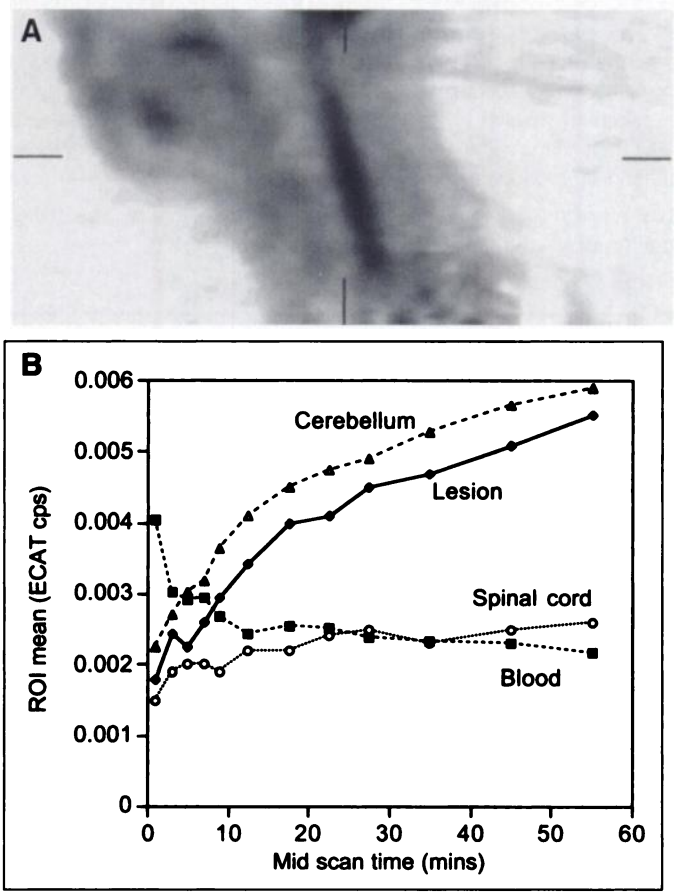

FIGURE 2. FDG PET imaging of cervical spine. (A) Summed (30–60 min postinjection) midsagittal FDG PET image data demonstrates focal elongated segment of markedly increased FDG uptake in midcervical spinal cord. (B) Time-activity curves demonstrating relationship of FDG uptake among lesion, blood (carotid arteries), unaffected spinal cord and cerebellum. Usual peak in blood curve at early times is reduced because of comparatively long 2-min frames. Note that the intense uptake of FDG in lesion is comparable to that in brain (cerebellum), and is factor of 2–3 higher than normal uptake in spinal cord.

DISCUSSION

We have demonstrated delineation of recurrent intramedullary PNET of the cervical spinal cord with FDG PET imaging.

FDG PET, which has been used extensively to differentiate post-treatment change and viable tumor in the brain (*13,14*), has not been routinely applied to image neoplastic involvement of the spinal cord. Evaluation of the spinal cord with PET is, in part, limited by scanner spatial resolution, with compromised sensitivity for the detection of hypermetabolic lesions smaller in size than approximately 2.5 times the scanner spatial resolution (*15,16*). However, current whole-body PET scanners with resolutions of 4–6 mm FWHM are well suited to extending imaging of CNS tumors below the neck.

Since the normal spinal cord is comprised of a relatively large amount of axonal white matter, it manifests lower FDG uptake than cortical brain tissue on PET imaging. The glucose metabolic rate of white matter is approximately one-third to one-fourth that of white matter (*17*); therefore, tumor-to-background contrast should be more favorable in the spinal cord than in cortical brain regions. This has been verified by Di Chiro et al. (*11*), who reported a glucose metabolic rate of 1.7 mg/100 gm brain tissue/min for normal spinal cord (compared to values of 6.0–7.0 for midbrain pons area) using a tomograph. Holtoff et al. (*9*) reported glucose metabolic rates that were mildly lower than those of cerebral gray matter in two cases of PNET. Tumor-to-white matter ratios in these two cases were approximately 1.9 and 1.1. Interestingly, this group reported glucose metabolic rates of nearly twice that of PNET in the histologically similar medulloblastoma. In accord with the findings of Holtoff et al. (*9*), the spinal cord PNET lesion in our case was hypermetabolic relative to the unaffected spinal cord but similar in FDG uptake to the cerebellum. Prior radiation therapy to the entire neural axis may have diffusely lowered baseline FDG uptake in all nontumor CNS tissue, further contributing to increased lesion-to-spinal cord contrast.

CONCLUSION

The most clinically useful role of FDG PET imaging in patients with CNS neoplasms has been in the diagnosis of suspected tumor recurrence. In this setting, CT or MRI may be indeterminant due to anatomical distortion from surgical-, radiation- and/or chemotherapy-induced changes (*18*). PET has been effectively used to noninvasively distinguish active tumor from post-treatment effects in the brain. This case report illustrates that, with the recent progress in PET technology, it is now feasible to use FDG PET in the evaluation of spinal cord neoplasms.

REFERENCES

1. Ishikawa M, Kikuchi H, Miyatake S, Oda Y, Yonekura Y, Nichizawa S. Glucose consumption in recurrent gliomas. *Neurosurgery* 1993;33:28–33.
2. Patronas NJ, Di Chiro G, Kufta C, et al. Prediction of survival in glioma patients by means of positron emission tomography. *J Neurosurg* 1985;62:816–822.
3. Alavi JB, Alavi A, Chawluk J, et al. Positron emission tomography in patients with glioma. A predictor of prognosis. *Cancer* 1988;62:1074–1078.
4. Hoffman JM, Lowe VJ, Brown M, Burger P, Hanson MW, Coleman RE. The prognostic and diagnostic usefulness of FDG-PET in primary brain tumor management [Abstract]. *J Nucl Med* 1993;34:37P.
5. Mineura K, Sasajima T, Kowada M, et al. Perfusion and metabolism in predicting the survival of patients with cerebral gliomas. *Cancer* 1994;73:2386–2394.
6. Rosenfeld SS, Hoffman JM, Coleman RE, Glantz MJ, Hanson MW, Schold SC. Studies of primary central nervous system lymphoma with fluorine-18-fluorodeoxyglucose positron emission tomography. *J Nucl Med* 1992;33:532–536.
7. Kuwabara Y, Ichiya Y, Otsuka M, et al. High ^{18}F-FDG uptake in primary cerebral lymphoma: a PET study. *J Comput Assist Tomogr* 1988;12:47–48.
8. Di Chiro G, Hatazawa J, Katz DA, Rizzoli HV, De Michele DJ. Glucose utilization by intracranial meningiomas as an index of tumor aggressivity and probability of recurrence: a PET study. *Radiology* 1987;164:521–526.
9. Holthoff VA, Herholz K, Berthold F, et al. In vivo metabolism of childhood posterior fossa tumors and primitive neuroectodermal tumors before and after treatment. *Cancer* 1993;72:1394–403.
10. Griffeth LK, Rich KM, Dehdashti F, et al. Brain metastases from non-central nervous system tumors: evaluation with PET. *Radiology* 1993;186:37–44.
11. Di Chiro G, Oldfield E, Bairamian D, et al. Metabolic imaging of the brain stem and spinal cord: studies with positron emission tomography using ^{18}F-2-deoxyglucose in normal and pathological cases. *J Comput Assist Tomogr* 1983;7:937–945.
12. Sasajima T, Mineura K, Itoh Y, et al. Spinal cord ependymoma: a positron emission tomographic study with (^{11}C-methyl)-L-methionine. *Neuroradiology* 1996;38:53–55.
13. Doyle WK, Budinger TF, Valk PE, Levin VA, Gutin PH. Differentiation of cerebral radiation necrosis from tumor recurrence by ^{18}F-FDG and ^{82}Rb positron emission tomography. *J Comput Assist Tomogr* 1987;11:563–570.
14. Glantz MJ, Hoffman JM, Coleman RE, et al. Identification of early recurrence of primary central nervous system tumors by ^{18}F-fluorodeoxyglucose positron emission tomography. *Ann Neurol* 1991;29:347–355.
15. Hoffman EJ, Huang SC, Phelps ME. Quantitation in positron emission CT: 1. Effect of object size. *J Comput Assist Tomogr* 1979;3:299–308.
16. Kessler RM, Ellis JR, Eden M. Analysis of emission tomographic scan data: limitations imposed by resolution and background. *J Comput Assist Tomogr* 1984;8: 514–522.
17. Mazziotta JC, Phelps ME, Plummer D, Kuhl DE. Quantitation in positron emission tomography: 5. Physical-anatomical effects. *J Comput Assist Tomogr* 1981;5:734–743.
18. Dooms GC, Hecht S, Brant-Zawadski M, Berthiaume Y, Norman D, Newton TH. Brain radiation lesions: MR imaging. *Radiology* 1986;158:149–155.

Investigation of Angiotensin II/AT$_1$ Receptors with Carbon-11-L-159,884: A Selective AT$_1$ Antagonist

Zsolt Szabo, Pan Fu Kao, H. Donald Burns, Raymond E. Gibson, Terence G. Hamill, Hayden T. Ravert, Sang Eun Kim, William B. Mathews, John L. Musachio, Ursula Scheffel and Robert F. Dannals

Division of Nuclear Medicine, The Johns Hopkins Medical Institutions, Baltimore, Maryland; and Department of Pharmacology, Merck Research Laboratories, West Point, Pennsylvania

Antagonists of the angiotensin II AT$_1$ receptor subtype have been recently introduced for treatment of arterial hypertension and for pharmacological studies of these receptors. The purpose of this work was to label such an antagonist with ^{11}C and test the applicability of the radioligand for PET studies. **Methods:** The potent and selective nonpeptide AT$_1$ antagonist L-159,884 was labeled with ^{11}C and injected intravenously into six dogs. Renal accumulation and kinetics of the radioligand were imaged with PET at baseline and after receptor blockade with 1 mg/kg MK-996. Time-activity curves were derived from the renal cortex and were analyzed by the Gjedde-Patlak plot to obtain the influx rate constant of the radioligand. **Results:** There was selective radioligand binding in the kidneys, mainly located in the cortex. Within the time interval between 95 and 115 min postinjection, the radioactivity retained in the kidneys was 109 ± 27 and 42 ± 4 nCi/ml/mCi of the injected dose for the control and inhibition studies, respectively. The influx rate constant of the radioligand decreased from a baseline of 0.0298 ± 0.0156 to a post-MK-996 value of 0.0098 ± 0.0052. **Conclusion:** These results demonstrate distinct binding of ^{11}C-L-159,884 in the renal cortex with a specific binding component suitable for quantitative PET imaging of angiotensin II/AT1 receptors.

Key Words: PET; kidney; carbon-11; substituted benzoyl sulfonamides; dogs; angiotensin receptors

J Nucl Med 1998; 39:1209–1213

Received Jan. 16, 1997; revision accepted Oct. 13, 1997.

For correspondence or reprints contact: Zsolt Szabo, MD, PhD, Division of Nuclear Medicine, The Johns Hopkins Medical Institutions, Nelson Building B1-119, 600 North Wolfe St., Baltimore, MD 21030.